Numerical Analysis of Injection Molding of Glass Fiber Reinforced Thermoplastics. Part 2: Fiber Orientation

JOSEPH P. GREENE

Body-In-White Center, A/MD-33
General Motors Corporation
Warren, Michigan 48090-9010

and

JAMES O. WILKES

Department of Chemical Engineering
The University of Michigan
Ann Arbor, Michigan 48109-2136

Numerical predictions of fiber orientation during injection molding of fiber-filled thermoplastics are compared to measurements. The numerical work successfully describes the flow of fiber-filled plastic during injection molding, using finite-difference solutions for the transport equations and marker particles to track the flow front. The flow is modeled as a 2-D, non-isothermal, free-surface flow with a new viscosity model dependent upon temperature, pressure, and fiber concentration. The fiber orientation is based upon solution to the Fokker-Planke equation. The comparison demonstrates fair agreement between predicted fiber orientation and experimental results for slow and fast injection speeds. For the slow speed case at 10 and 20 wt% fibers, the numerical and experimental works show that the fibers are more random at the flow front than at the centerline, and that the fibers become more aligned as they flow from the gate to the midstream region. At fast injection speeds, the agreement between the numerical and experimental works is not as good as at slow injection speed. Possible explanations for the discrepancies are that the flow is assumed to be simple shear when injection molding is known to be a pressure-driven flow, the fibers have an initial orientation for the runner rather than the assumed random orientation, the fibers that were displayed from the camera were more oriented just behind the flow front (owing to the fast injection speed), and the orientation requires more than a 2-D video image to represent a 3-D fiber orientation.

INTRODUCTION

Mold-filling analysis of injection molding has been of considerable research interest over the past twenty years. Injection of a plastic melt into a cool die cavity generally involves three flow regions (*Fig. 1*): the gate region, the fully developed region, and the fountain region.

In a typical end-gated, thin-walled cavity, the gate region is characterized by radial flow, the fully developed region by a dominant parallel-velocity component, and the fountain region by a free-surface flow. The objective of the flow analysis is to obtain pressure and velocity distributions for a thermoplastic in a closed cavity, by solving the momentum and energy transport equations with an appropriate constitutive equation.

Previous researchers modeled the flow during injection molding as a Newtonian material in a fully developed one-dimensional flow. In particular, Williams and Lord (1) and Huang *et al.* (2) expanded to two dimensions and to include the thermal and pressure effects during the filling of the gate and the fountain regions. Harry and Parrott (3) and Berger and Gogos (4) developed appropriate constitutive equations to describe the shear, thermal, and pressure influences upon the viscosity. Several finite-difference codes are available to solve the coupled momentum and energy

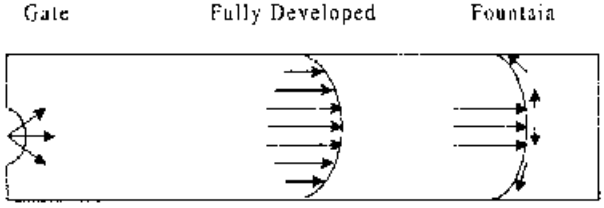

Fig. 1. Flow regions during injection molding.

transport equations in the three flow regions, e.g., Moldflow (5) and C-Flow (6).

Few researchers have incorporated fiber-filled polymer melts into the flow analysis, due to the absence of an appropriate constitutive equation. The rheological equations of state for fiber suspensions are based upon the orientation of the fibers. This orientation is represented by the fourth-order dot product of the orientation vector, **p**, and based upon Batchelor's bulk stress expression. Kamal and Mutel (7) approximated the fourth order tensor for simple flow systems. Folgar and Tucker (8) developed an empirical diffusion model that predicted the inter-fiber contact forces based upon hydrodynamic friction between moving intersecting particles. The forces transmitted across the contact point was proportional to the relative velocity between the two particles at that point. The orientation tensor was formed by taking the dyadic product of the vector, **p**, with itself and integrating the product times the distribution function. The odd order tensors are zero since the distribution function is even. An infinite set of even-order tensors is formed. The stress tensor is represented by a second-order or a fourth-order rank tensor with an added interaction coefficient $\mathbf{C_I}$ that takes into account the fiber interaction. The fourth-order rank tensor is computationally intensive. Tucker (9) approximated the second-order rank tensor with a summations of the double dot product of the orientation vector. Advani and Tucker (10) treated the orientation of the fibers based upon a three dimensional, second-order rank tensor. Bay and Tucker (11) found that the theory did not accurately reflect data for concentrated solutions.

Recently, Ausias *et al.* (12) used a simple approach to describe the rheology of semi-dilute suspensions of fibers with a second-order tensor. The fiber evolution equation is based upon the motion of a single ellipsoid in a Newtonian fluid under simple shear flow from Jeffery (13). The model contains only one adjustable parameter. The transient relative viscosity is a function of strain and not time or shear rate separately. The model gives reasonable predictions of experimental data. Other researchers (14, 15) based the prediction of fiber orientation upon the second order tensors with mixed results.

This research predicts the fiber orientation during injection molding of a small plaque part with the fibers orienting as a function of total strain. The fibers effects on viscosity are taken into account with a fiber concentration parameter. This work is the last portion of a research project by Greene (16) in the study of fiber orientation during flow of fiber-filled thermoplastics. The research work predicts the flow of fiber-filled thermoplastics by incorporating the energy equation into the flow program, by incorporating the shear rate, temperature, and pressure effects on the viscosity, and, lastly, by incorporating fiber-orientation effects on the viscosity and the flow field. This work is preceded by an investigation by Greene and Wilkes (17) into the effects the fibers have on the molecular weight and steady-state viscous properties of three thermoplastics materials and by a numerical analysis study, by the same authors (18), that predicts flow and pressures during injection molding. The numerical investigation incorporates a modified Carreau model into a commercial mold-filling analysis package, FLOW-3D, that utilizes finite-difference solutions for the transport equations and marker particles to track the flow front. The fiber orientation is found from the solution of the Fokker-Plank equation. The details of the numerical work including descriptions of the numerical analysis and rheological coefficients of the materials are given in the previous work by Greene and Wilkes (18) and will not be presented here.

Fiber-Orientation Calculation

Once the flow dynamics have been determined and the flow and pressure distributions found, the fiber orientation can be calculated based upon fiber concentration and total strain. The probability distribution function, $\psi(\mathbf{p}, t)$, can be found for simple-shear flow according to the following:

$$\psi(\mathbf{p}, t) = \frac{1}{4\pi}\left[\frac{p_1^2 - 2\gamma p_1 p_2 - (1+\gamma^2)p_2^2 + p_3^2}{p_1^2 + p_2^2 + p_3^2}\right] \tag{1}$$

where γ is the total strain, defined for m time steps as the sum of shear rate in the time step multiplied by the time increment in the time step, $\gamma = \sum_{i=1}^{m} \dot{\gamma}_{ijx}\Delta t_i$.

The fiber-orientation calculations as well as the modified viscosity relationships for temperature, pressure, and fiber concentration were added to the computer program.

Fiber Orientation

Fiber orientation is found by conserving the fibers in the orientation space, **p**. The solution for the fiber-orientation-distribution function, $\psi(\mathbf{p}, t)$, is found using the Fokker-Plank solution to the conservation of fibers in the orientation space as:

$$\psi(\mathbf{p}, t) = \frac{1}{4\pi}(\Delta^{-1} \cdot \Delta : pp)^{3/2} \tag{2}$$

where $\Delta = \mathbf{E}^{-1}$ is the deformation gradient defined previously, and **p** is the orientation of the fiber at time t. The orientation of the fiber is determined once the velocity field and hence the deformation gradients are

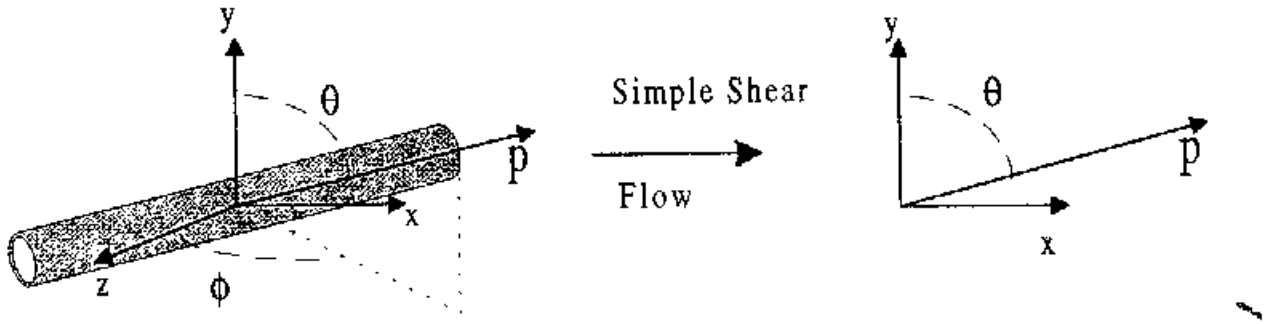

Fig. 2. Fiber orientation vector **p** *for simple shear flow.*

Fig. 3. Fiber orientation measurement process.

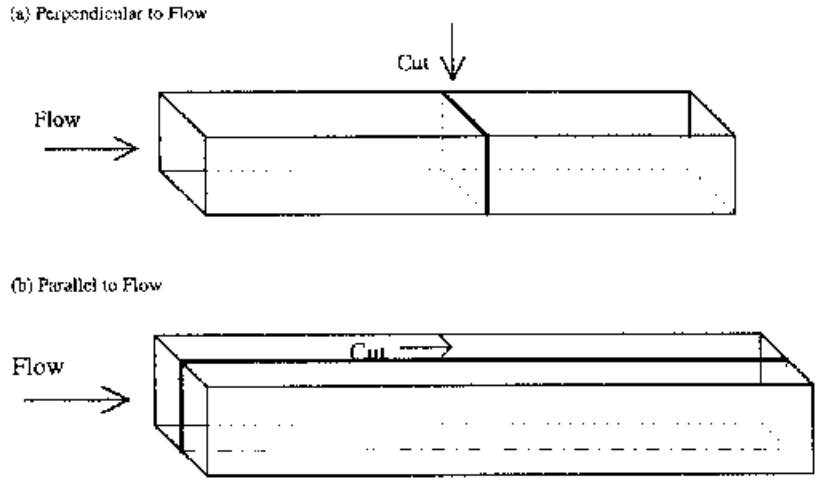

Fig. 4. Fiber orientation: (a) perpendicular and (b) parallel to flow direction.

determined, which for simple shear flow is:

$$\psi(p, t) = \frac{1}{4\pi}\left[\frac{p_1^2 - 2\gamma p_1 p_2 + (1 + \gamma^2)p_2^2 + p_3^2}{p_1^2 + p_2^2 + p_3^2}\right] \qquad (3)$$

The numerical predictions calculate the probability that a fiber is at orientation **p** at time t based upon the total strain, γ, that the fiber has experienced. The orientation vector for simple shear flow is shown in *Fig. 2*.

In spherical coordinate system the orientation vector, **p**, is given by:

$$\mathbf{p} = \begin{pmatrix} p_1 \\ p_2 \\ p_3 \end{pmatrix} = \begin{pmatrix} \sin\phi \sin\theta \\ \cos\theta \\ \cos\phi \cos\theta \end{pmatrix} = \begin{pmatrix} \sin\theta \\ \cos\theta \\ 0 \end{pmatrix}$$

During injection molding of a polymer in a thin-walled cavity, the fibers again will align in the direction of flow, namely, $\theta = 90°$. The following analysis assumes that the flow can be represented as simple shear where the x-component of the velocity (with x being the flow direction) has the largest gradient in the perpendicular direction (here, the y-direction). This contrasts with a pressure driven flow during injection molding, and could be a source of error in the analysis. The flow analysis shows a small y velocity component when compared to the x (flow direction) velocity component. FLOW-3D was modified by incorporating a total strain variable into the program. Since the distribution function only requires a total strain at each location, the modification was only required in the subroutine that calculated the shear rate. The total strain then was the sum of the total strain from the previous-time step and the strain from the current-time step. The current-time-step strain was the product of the shear rate and the time step, *Eq 4*.

$$\gamma_{new} = \gamma_{old} + \dot{\gamma}\Delta t \qquad (4)$$

The numerical analysis then results in a printout of the total strain at several locations, i.e., five equal increments from the centerline ($y = 0$) to the wall ($y =$

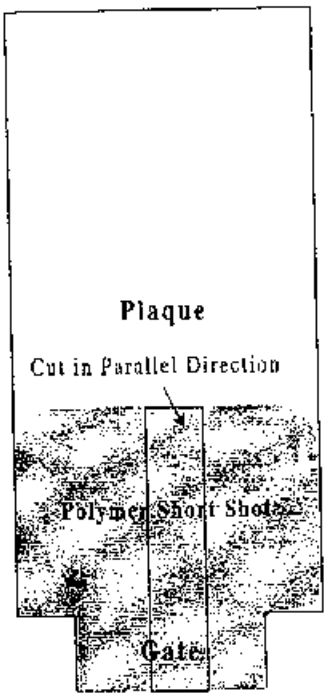

Fig. 5. Fiber orientation for the plaque in the parallel to flow direction.

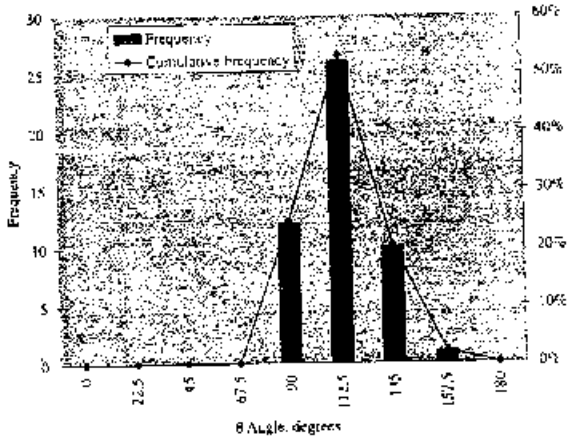

Fig. 6. Case 1: Experimental fiber-orientation distribution at the gate location.

0.15 cm). At the wall a no-slip boundary condition exists, so the velocity is zero.

Since most of the orientation occurs in the thickness direction, the flow is computed in two dimensions, neglecting the width direction. The analysis is for an incomplete fill with the flow terminating at ~50% of the length of the full part. The analysis calculates fiber orientation at the gate, midstream, and flow-front locations. For the midstream and flow-front locations, the total strain is determined based upon the fill time. For the gate location, the total strain is based upon the time as the flow front moves one cell past the gate. The results are compiled for 10 and 20 wt% short-fiber-reinforced polypropylene and at slow and fast fill.

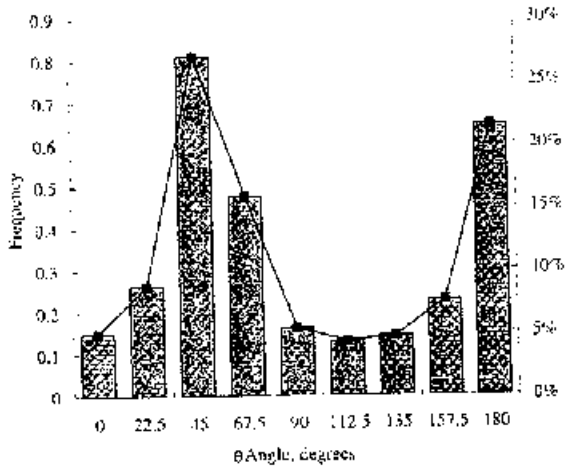

Fig. 7. Case 1: Predicted fiber-orientation distribution at the gate location.

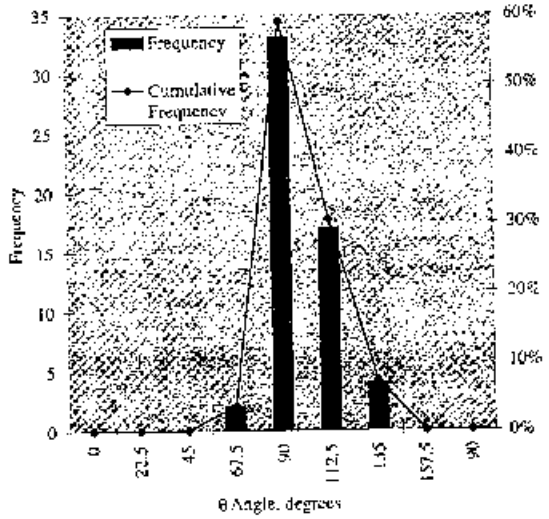

Fig. 8. Case 1: Experimental fiber-orientation distribution at the midstream location.

EXPERIMENTAL MEASUREMENTS OF FIBER ORIENTATION

The fiber orientation work measures orientation in an injection-molded short-shot plaques. The short shots were generally filled just past the mid-stream pressure transducer. The plaques were injection molded at 10 and 20 wt% glass fibers for slow and fast injection speeds. The plaques were then used to cut a microtome test sample that was then optically analyzed for fiber orientation. The plaques were sectioned in two different directions at the gate, midstream, and flow-front locations. The steps in the fiber-orientation-measurement process consist of five major areas and five instruments. The process is described in the next section and illustrated in *Fig. 3*.

Step 1: Injection Molded Plaque Preparation

The first step is to prepare the test sample for cutting by injection molding the intended part that can be

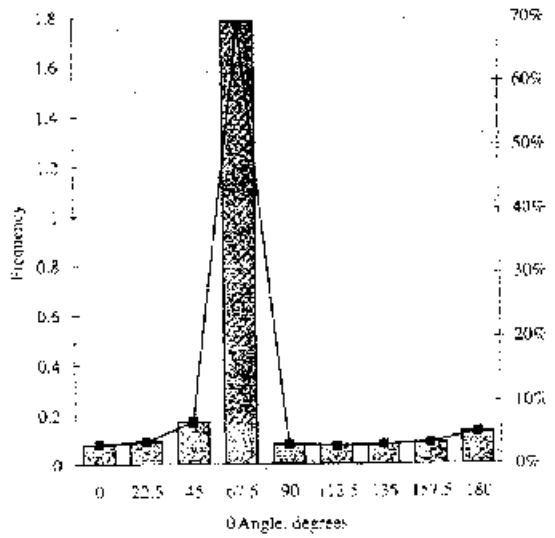

Fig. 9. Case 1: Predicted fiber orientation distribution at the midstream location.

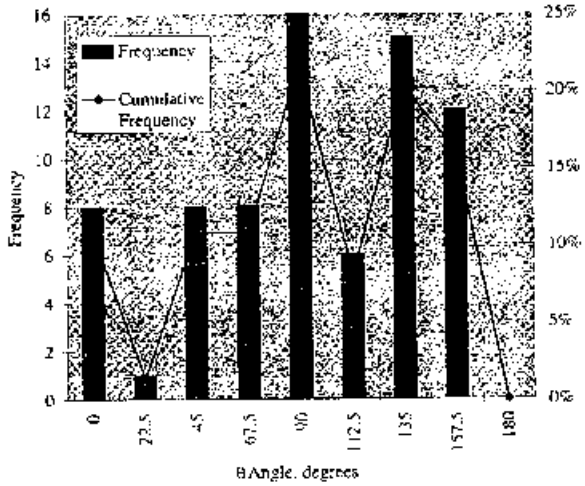

Fig. 10. Case 1: Experimental fiber orientation distribution at the flow-front location.

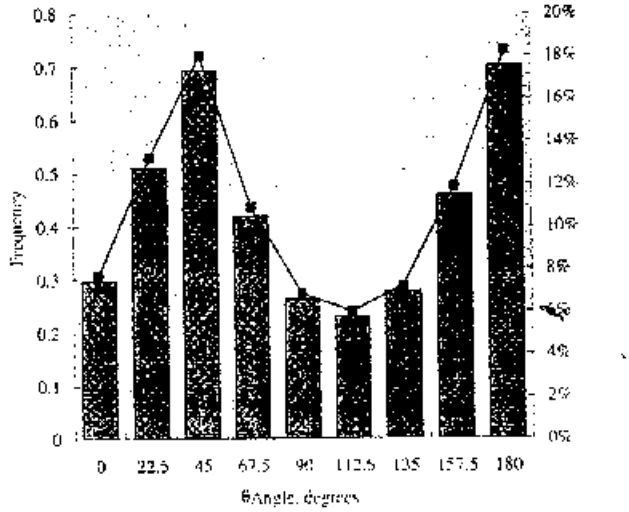

Fig. 11. Case 1: Predicted fiber-orientation distribution at the flow-front location.

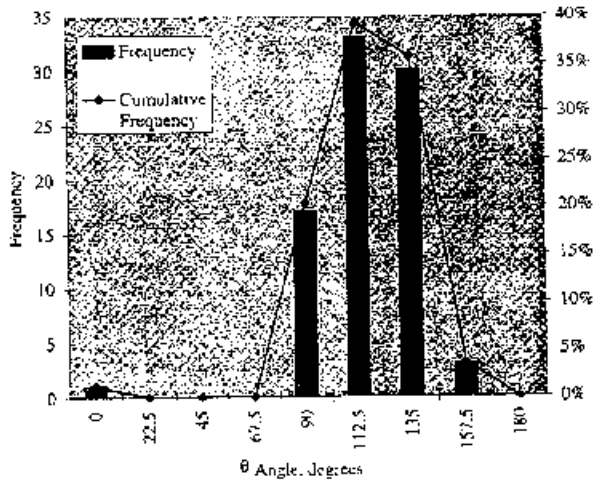

Fig. 12. Case 2: Experimental fiber orientation distribution at the gate location.

a production plastic part, tensile bar, or a test plaque. A New Britain, model 75-TP, single-screw-injection-molding machine is used during the research. The resin is injected into a 7.55 by 15.1 by 0.3 cm cavity via a runner system. The test sample is then sectioned to fit into the fixture apparatus of the microtome cutter that will be described in the next section.

Step 2: Polycut Microtome Procedure

The test plaque is cut into microtome samples at a prescribed thickness, in this case 90 μm, to provide a specimen that can be optically measured. A Reichert-Jung heavy-duty microtome was used for this procedure. The POLYCUT S is a universal heavy-duty microtome for both biomedical and industrial applications. Large specimens up to 25 × 20 cm and hard materials such as bone or plastic can be sectioned. The POLYCUT has a wide range of specimen holders and knife stages for industrial applications. The specimen is rigidly held into place on the stage that is adjustable in height and orientation with respect to the blade. The stage then passes under a fixed knife blade at a constant rate. The plaque sample is thinly sliced as the stage moves under the blade into shavings at a prescribed thickness, and placed between two glass slides. The plaque sample is positioned in the POLYCUT fixture to get cuts at two different sample directions, one perpendicular to flow and one parallel to flow, as shown in *Fig. 4*.

The two different cut directions enable an analysis of the flow characteristics of the fibers during injection molding. The perpendicular direction sample provides information of the orientation state as influenced by the top and bottom walls in the thickness direction, and the influence of the side walls in the width direction. The slices at the entrance, midstream, and the flow front locations can show the influence of the walls on the fiber orientation in the plaque. The parallel

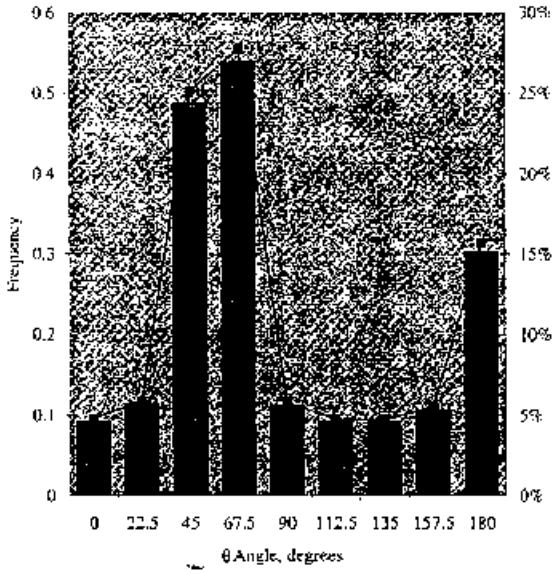

Fig. 13. Case 2: Predicted fiber-orientation distribution at the gate location.

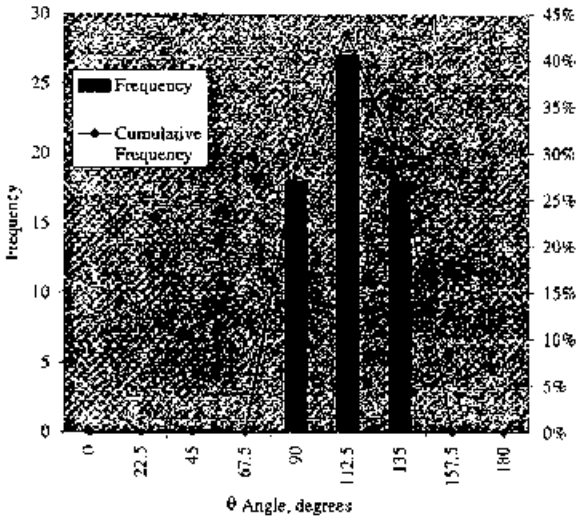

Fig. 14. Case 2: Experimental fiber-orientation distribution at the midstream location.

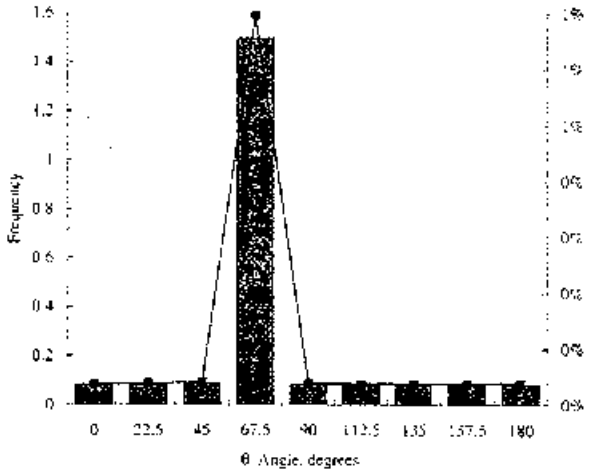

Fig. 15. Case 2: Predicted fiber orientation distribution at the midstream location.

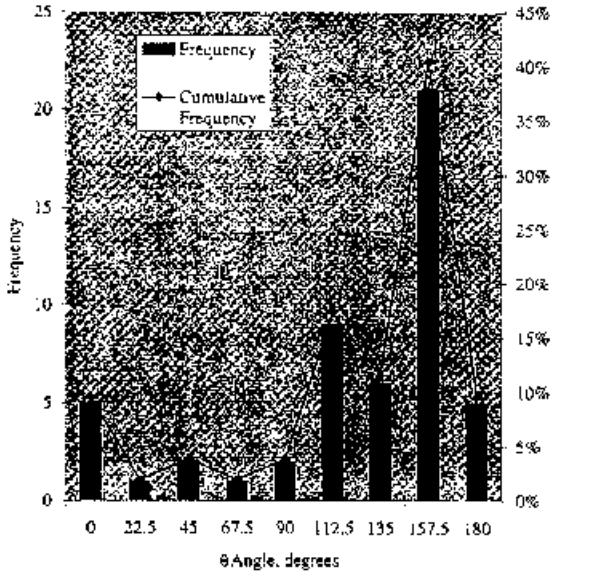

Fig. 16. Case 2: Experimental fiber-orientation distribution at the flow-front location.

direction sample, *Fig. 5*, provides the fiber orientation information as the fibers proceed from the gate to the midstream and finally to the flow front. The influences of the top and bottom walls on the fiber orientation will be apparent. The width direction will not be of importance since the plaque sample was sectioned at the centerline of the part. The orientation in the parallel direction was calculated during the numerical analysis after the fluid velocities, pressures, temperatures, and shear strains are calculated.

Step 3: Optical Microscope Measurements

An optical microscope is used to analyze the fiber orientation state of the microtomed sample. In particular, a Nikon Microphot-FX instrument was used to examine the test sample. The Nikon unit is composed of a microscope with an eyepiece, 35 mm camera, color video camera, and several objectives. The magnification was 40×. The color video camera, CCD camera module, displayed the camera to a monitor and to a Macintosh II computer. The sample image was recorded with the 35 mm camera.

Step 4: Image-Capture Measurements

The image projected from the video camera is then processed into a sharper image by using a software package, MICRO-TOME, which uses the nearest-neighbor algorithm to remove haze from images. It does this by calculating the point spread function associated with the scanned data and mathematically removing the haze from each image. The output is saved in a MIC file format. The image file can be deconvoluted as well. The file format is then converted to

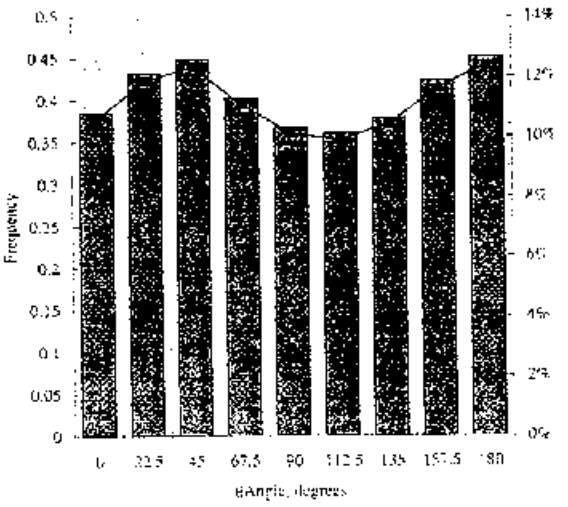

Fig. 17. Case 2: Predicted fiber-orientation distribution at the flow-front location.

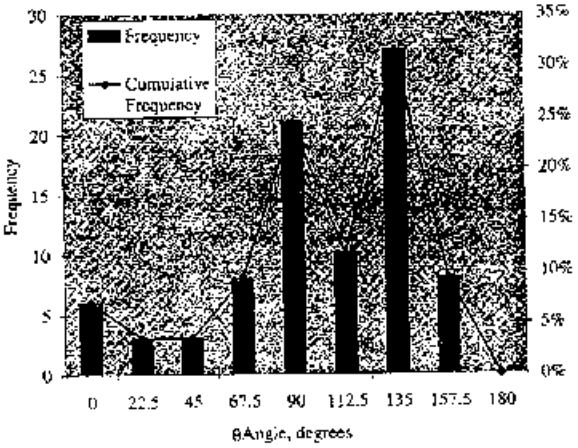

Fig. 18. Case 3: Experimental fiber-orientation distribution at the gate location.

a TIFF format by using Image Analyst software. The software allows the integration of video images with computer-based applications by exporting the image into a TIFF format. The image must be modified to compensate for the fact that the fiber and the resin matrix have similar gray tones, with the fibers appearing translucent. The translucent fibers are not easily measured by the fiber-orientation equipment, and were therefore darkened by using the line draw function of the software while using the image from the video camera as a guide. The output files of the enhanced pictures are given in the **Appendix**.

Step 5: Fiber Orientation Measurements

The last stage is the actual measurements of the fiber orientation from the output files by using the Quantimet 570 from Leica (19). The Quantimet 570 embodies image processing and morphological techniques, built into a programmable gray-tone image processor. Actually, two 386 processors are used for the image analysis, numerical computation, and color

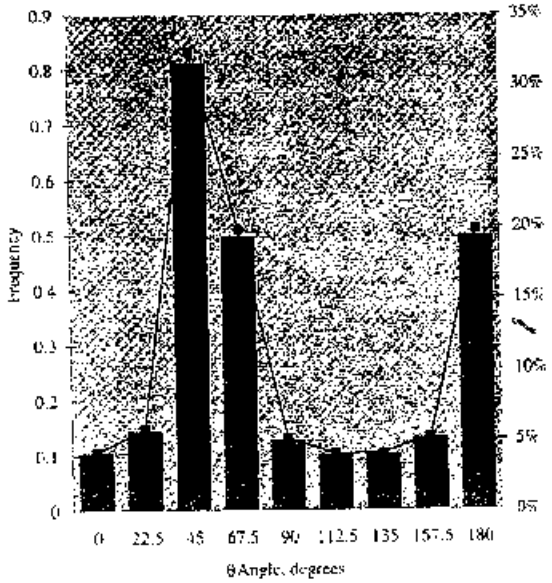

Fig. 19. Case 3: Predicted fiber-orientation distribution at the gate location.

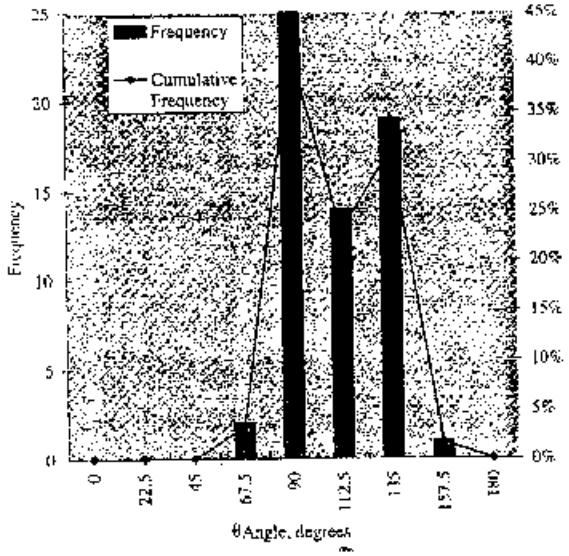

Fig. 20. Case 3: Experimental fiber orientation distribution at the midstream location.

displays. The Quantimet 570 incorporates a new generation of gray-scale image processing software, based upon the mathematical morphology techniques developed by the Centre de Morphologie Mathématique at the Ecoles des Mines, Paris, in close conjunction with Cambridge Instruments (20).

According to Serra (21), image analysis based upon mathematical morphology simplifies the image for segmentation and measurement, and is achieved by rapid modification of the image pixels according to the gray values of their neighbors. The transformation, as presented by Beucher and Serra (22) and Beucher and Vincent (23), is controlled by the action of a structuring element centered on each pixel. Quantimet 570 begins the analysis process by applying matrix shad-

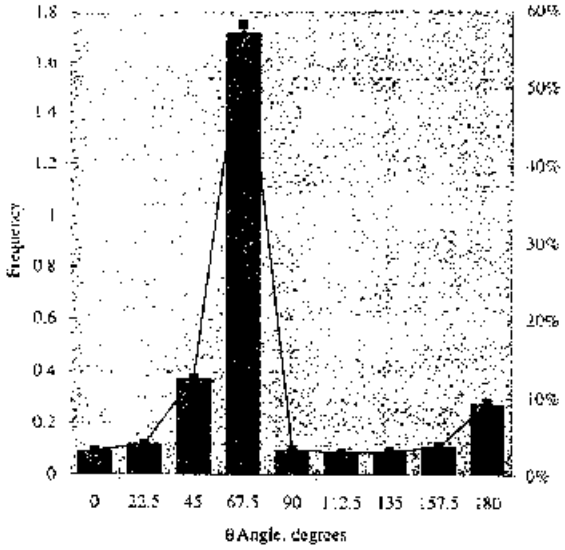

Fig. 21. Case 3: Predicted fiber-orientation distribution at the midstream location.

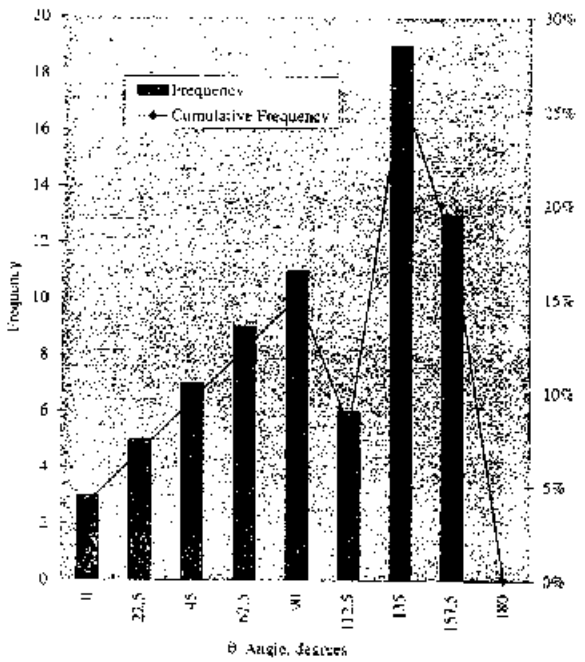

Fig. 22. Case 3: Experimental fiber-orientation distribution at the flow-front location.

ing correction and digitizing the image into 256 gray levels. Each frame is cleaned up by successively averaging a series of video images to filter out background noise and then saved.

The saved image is then manipulated by a gray-tone image processor, based upon Programmable Logic Cell Array technology, and optimized to handle morphological transformations. Some examples of the morphological transformations are *top hat, delineate, gradient, gray build, maxima/minima, hit or miss, amend, watershed, prune, skiz, identify points, segment, label,* and *distance*. In addition to the fiber orientation, the software calculates the fiber length distributions. The output is sent to a Lotus file.

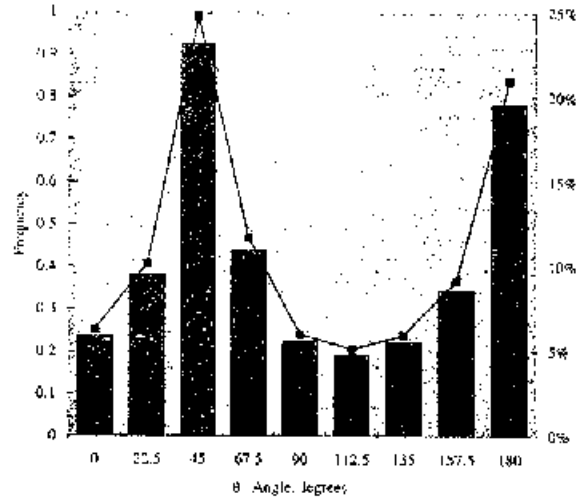

Fig. 23. Case 3: Predicted fiber-orientation distribution at the flow-front location.

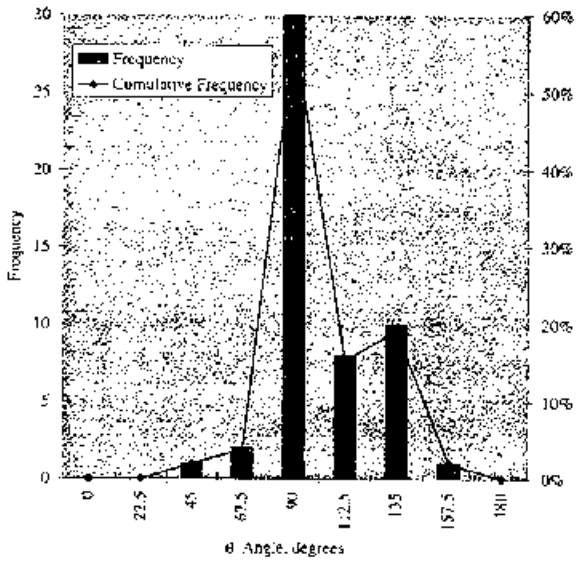

Fig. 24. Case 4: Experimental fiber-orientation distribution at the gate location.

The fiber orientation was measured for the 10 and 20 wt% short fiber at slow and fast injection speeds. Sample slices were taken at the gate, midstream, and flow front locations for the perpendicular direction. As a comparison, the sample slices for the parallel direction were taken at the centerline location ($y = 0$) and included the gate location at one end and the flow-front location at the other end of the same sample. The fiber-orientation results are presented and compared to numerical predictions. The fiber orientation for the direction perpendicular to flow is given for three areas, namely the gate, the midsection, and the flow front. The gate location in the perpendicular direction is located ~5 mm from the edge of the sample, in order to reduce any effects from the sample cut. Similarly, the

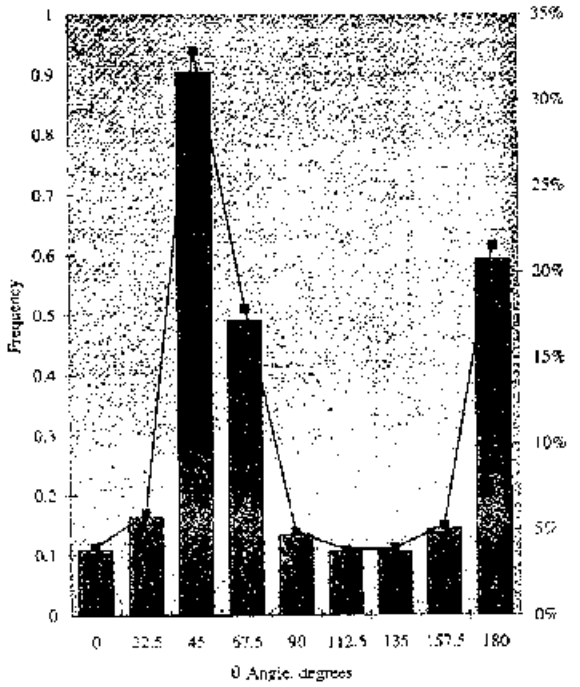

Fig. 25. Case 4: Predicted fiber-orientation distribution at the gate location.

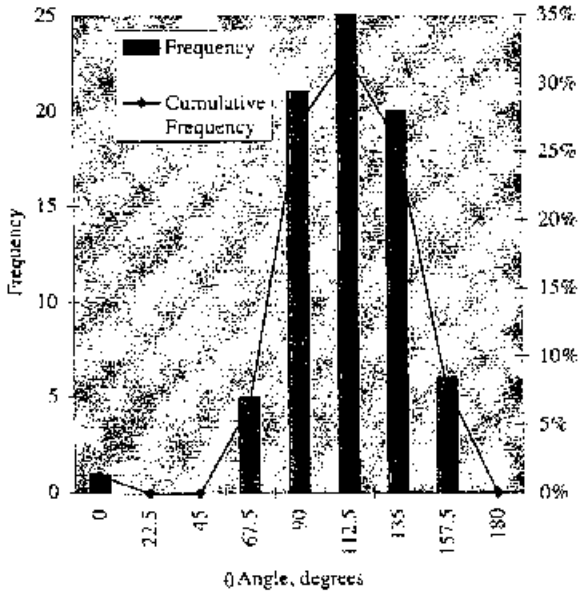

Fig. 26. Case 4: Experimental fiber-orientation distribution at the midstream location.

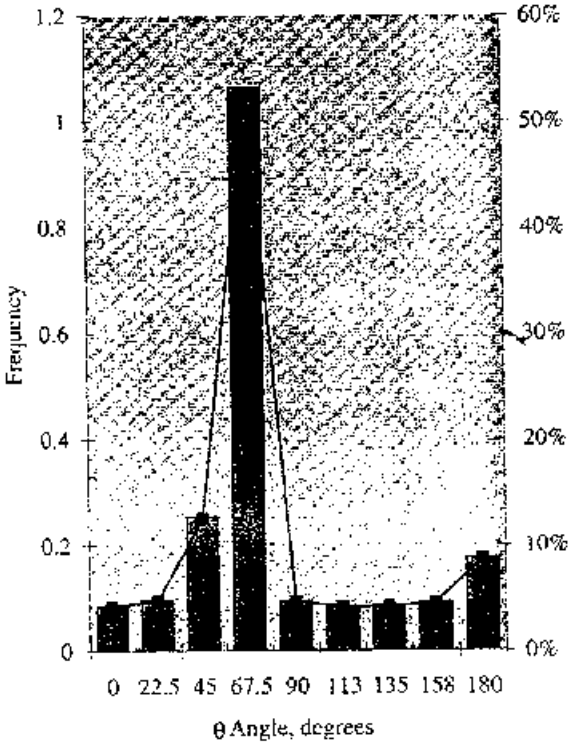

Fig. 27. Case 4: Predicted fiber-orientation distribution at the midstream location.

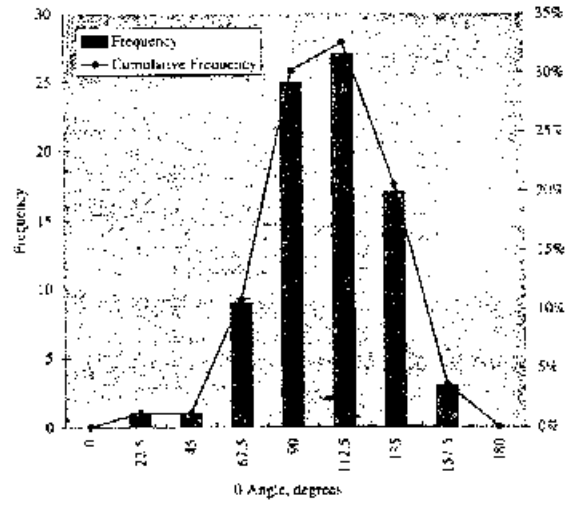

Fig. 28. Case 4: Experimental fiber-orientation distribution at the flow-front location.

flow-front location is ~2 mm from the edge, in order to get a crisp image. The midstream location is approximately half-way from the gate to the flow front. The measurement technique was limited by the assumption that the 3-D image can be represented with a 2-D video image. Some of the fibers, especially at the flow front, were out of the focus plane (pointing at the camera) and thus were not measured. Thus, some of the flow-front orientation results appear to be more random than they are. The software company is continuing to work on this problem. The data presented in the following figures are from one sample that gave the most crisp image, and typically had over 100 fibers per sample. The number of fibers at a certain orientation are called the *frequency*. The frequency divided by the total number of fibers and times 100 is defined as the *percentage* of fibers at that orientation angle, θ. The bar in the following figures denotes the frequency and the line denotes the percentage. The orientation is with respect to the perpendicular-to-flow direction and represented by the angle θ, (refer to *Fig.* 2).

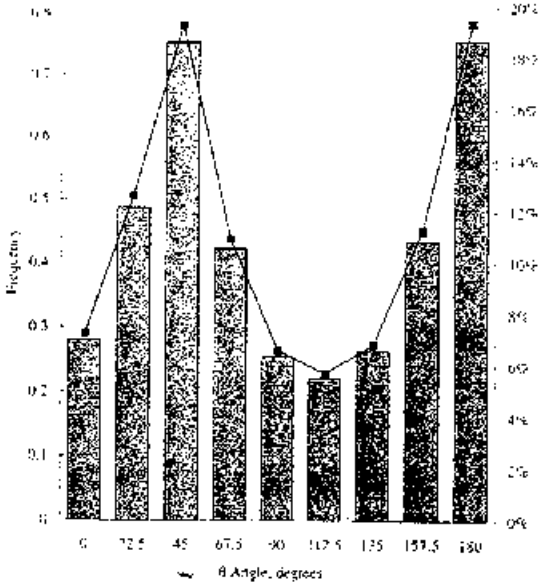

Fig. 29. Case 4: Predicted fiber-orientation distribution at the flow-front location.

COMPARISON OF EXPERIMENTAL TO PREDICTED FIBER ORIENTATION

The definition of the orientation angle is different for the two procedures. The numerical calculations predict the angle, θ, with reference to the normal-to-flow direction as explained in *Fig. 8*. The experimental procedure measures the orientation with respect to the flow direction, and hence is at an angle 90° relative to the numerical predictions. For comparison purposes, the experimentally measured orientation angle was translated to the same angle, θ.

Predicted Fiber Orientation for Simple-Shear Flow

The predicted fiber orientation for simple-shear flow using the modified, FLOW-3D computer program. The orientation data from the computer program, though, is calculated at five sections in the thickness direction. To be consistent with the experimental data graphs, the orientation results from the different locations in the thickness direction are combined onto one distribution graph for the x-location, e.g., gate, midstream, or flow-front location. The probability distribution is converted to a frequency distribution by computing the sum of the probabilities that the fiber is at an angle, q, for strains through the thickness, g at the centerline to g at the wall, and by computing the sum of probabilities for all angles of orientation, $\theta = 0°$ to 180°. The Dinh-Armstrong theory denotes that the sum of the probabilities for all of the orientation angles ($\theta = 0°$ to 180°) is equal to 1 for a given time (or strain). Note, that in our case, the sum of probabilities is not equal to unity since it is computed by summing the strains at various thickness locations, hence different times. For both the measured and predicted techniques, the sum of all fraction of fibers adds up to 1. The formula for computing the fraction of fibers $g(\theta)$, for the measured orientation is given in *Eq 5*, and for the predicted fraction of fibers is given in *Eq 6*. These fractions are multiplied by 100 to give the percentage of fibers at the orientation angle.

$$g(\theta) = \frac{N_i}{\sum_{i=1}^{n} N_i} \tag{5}$$

Here, N_i is the number of fibers, or frequency, at the orientation angle θ. The denominator is the total number of fibers.

$$g(\theta) = \frac{\sum_{j=1}^{5} \psi(\theta, \gamma_j)}{\sum_{i=1}^{n} \sum_{j=1}^{5} \psi(\theta, \gamma_j)} \tag{6}$$

Here, the numerator is the number of fibers at the five strain locations with an orientation θ, and the denominator is the total number of fibers at the five strain locations with all orientation angles ($\theta = 0$ to 180°).

The comparisons between the experimental and numerical work of fiber orientation in the *parallel direction* are given at the gate, midstream, and flow-front locations for four different conditions. Case 1, *Figs. 6* through *11*, is polypropylene with 10 wt% fibers at slow injection speed. Case 2, *Figs. 12* through *17*, is polypropylene with 10 wt% fibers at fast injection speed. Case 3, *Figs. 18* through *23*, is polypropylene with 20 wt% fibers at slow injection speed. Case 4, *Figs. 24* through *29* is polypropylene with 20 wt% fibers at fast injection speed. The experimental work is given first followed by the numerical predictions.

The orientation results from the previous graphs generally demonstrate that the fibers become more aligned as the flow progresses from the gate to the midstream and until the flow front is reached. At the flow front the fibers become more random because of the fountain effect. The orientation at the slow injection speed, Case 1 and Case 2, have better agreement of experimental to predicted results than the fast injection speed cases. In all four cases the measured orientation at the gate location is not random but has some orientation. Obviously, the fibers are somewhat aligned in the runner system, in contrast to an assumption of the Dinh-Armstrong theory and the numerical analysis. To correct this, the analysis would have to model the flow in the runner in addition to the gate and the cavity. This would be difficult with the FLOW-3D software since the runner is modeled in cylindrical coordinates and the gate and the cavity are modeled in rectangular coordinates. Another possible solution would be to put in an initial orientation vector, $\mathbf{p}_0$, at the gate location. This would require a new solution to the Fokker-Planck equation for an initial orientation state using the method of characteristics. Again this would be better left for future researchers.

The disagreement at the flow-front location between the experimental and numerical predictions is most pronounced for the fast injection speed cases. For the fast-speed case, *Fig. 16* and *Fig. 28*, the flow-front appears to have equal orientation to the midstream

location. Possibly, the fibers that were displayed from the camera were more oriented just behind the flow front (due to the fast injection speed) than the slow-fill case. Thus, the sample area was too wide and included more than the flow-front location. Another possible explanation for the discrepancies is that the flow is assumed simple shear when injection molding is known to be pressure-driven flow.

CONCLUSIONS

Numerical predictions of fiber orientation during injection molding of fiber-filled thermoplastics are compared to experimental measurements. Additionally, experimental methods and equipment used for fiber orientation measurements are presented. The fiber orientation is calculated based upon solution to the Fokker-Planke equation. The simplified model allows for quick calculation of the fiber orientation as a function of total strain. The comparison demonstrates fair agreement between predicted fiber orientation and experimental results for slow and fast injection speeds. For the slow speed case at 10 and 20 wt% fibers, the numerical and experimental works show that the fibers are more random at the flow front than at the centerline, and that the fibers become more aligned as they flow from the gate region to the midstream region. At fast injection speeds, the agreement between the numerical and experimental works is not as good as at slow speeds. Possible explanations for the discrepancies are that the flow is assumed simple shear when injection molding is known to be pressure-driven flow, the fibers have an initial orientation for the runner rather than the assumed random orientation, the fibers that were displayed from the camera were more oriented just behind the flow front (owing to the fast injection speed), and the orientation requires more than a 2-D video image to represent a 3-D fiber orientation.

APPENDIX
Fiber Orientation Results: TIFF Files

The graphic images given in the following pages are the files that were measured for fiber orientation. The material type, flow location, and flow orientation are given at the top of each image. The flow in all cases is from the right to the left. The top of the image is the mold wall and the bottom of the image is the mold wall.

Polypro 10% short fiber fast fill at the gate and perpendicular to flow

Polypro 10% short fiber fast fill at the mid-stream and perpendicular to flow

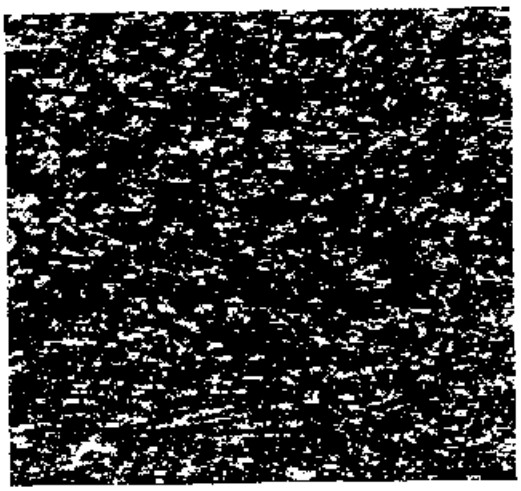

Polypro 20% short fiber slow fill at the flow front and parallel to flow

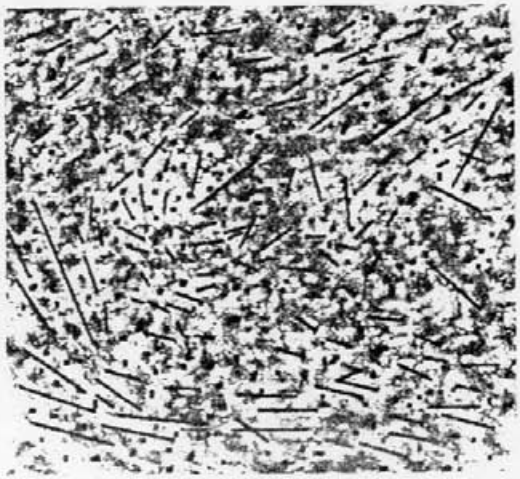

Polypro 20% short fiber fast fill at the gate and parallel to flow

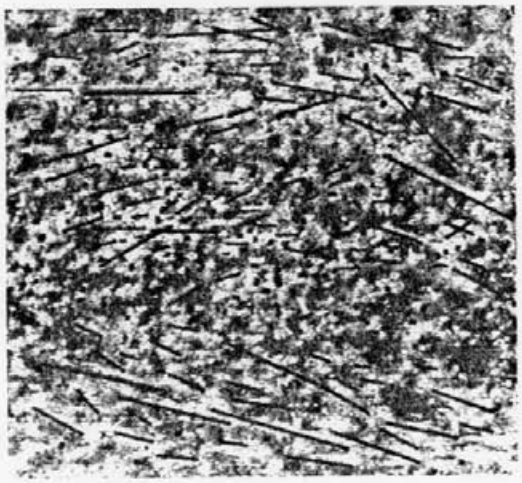

Polypro 20% short fiber fast fill at the mid-section and parallel to flow

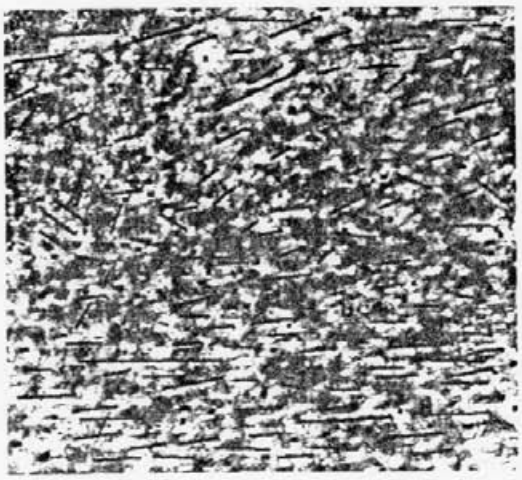

Polypro 20% short fiber fast fill at the flow front and parallel to flow

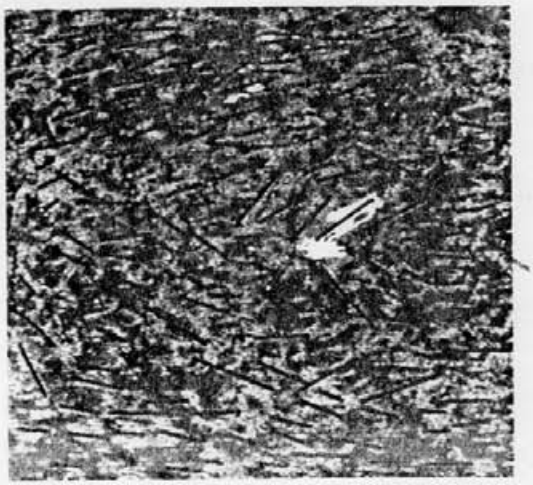

REFERENCES

1. G. Williams and H. Lord, *Polym. Eng. Sci.*, **15,** 569 (1975).
2. C. Gogos, C. Huang, and L. Schmidt, *Polym. Eng. Sci.*, **26,** 1457 (1986).
3. D. Harry and R. Parrott, *Polym. Eng. Sci.*, **10,** 209 (1970).
4. J. Berger and C. Gogos, *Polym. Eng. Sci.*, **13,** 102 (1972).
5. C. Austin, Technical Report, Moldflow pty., Ltd., Kilsyth, Victoria, Australia (1987).
6. C-Flow is a flow package from AC Technology Inc. Ithaca, New York.
7. M. Kamal and A. Mutel, *Polym. Compos.*, **10,** 343 (1989).
8. F. Folgar and C. Tucker, *J. Rheol.*, **28,** 207 (1984).
9. C. Tucker, *Proc. Manuf. Int. '88*, **IV,** 95 (1988).
10. S. Advani and C. Tucker, *J. Rheol.*, **31,** 751 (1987).
11. S. Bay and C. Tucker, *Polym. Compos.*, **13,** 332 (1992).
12. G. Ausias, J. Agassant, and J. Vincent, *J. Rheol.*, **36,** 4 (1992).
13. G. Jeffery, *Proc. R. Soc.*, **A102,** 161 (1922).
14. G. Libscomb, M. Denn, D. Hur, and D. Boger, *J. Non-Newt. Fluid Mech.*, **26,** 297 (1988).
15. M. Becraft and A. Metzner, *J. Rheol.*, **36,** 1 (1992).
16. J. Greene, PhD thesis, The University of Michigan (1993).
17. J. Greene and J. Wilkes, *Polym. Eng. Sci.*, **35,** 1679 (1995).
18. J. Greene and J. Wilkes, *Polym. Eng. Sci.*, accepted for publication.
19. Leica Inc., 111 Deer Lake Road, Deerfield, Illinois 60015; (708) 405-0123.
20. G. Matheron, *Elements pour une Thorie des Milieux Poreux*, Masson, Paris (1967).
21. J. Serra, *Image Analysis and Mathematical Morphology*, Vol. 2, Theoretical Advances, Academic Press, London (1988).
22. S. Beucher and J. Serra, *European Symposium on Stereology*, Ljubljana, Yugoslavia (1981).
23. S. Beucher and L. Vincent, *Journal de Microscopie et de Spectroscopie Electronique*, April 1989.

Revised December 1996